

Swarm-derived indices of geomagnetic activity

Constantinos Papadimitriou^{1,2,3}, Georgios Balasis¹, Adamantia Zoe Boutsis^{1,2},
Alexandra Antonopoulou¹, Georgia Moutsiana², Ioannis A. Daglis^{2,4,1}, Omiros
Giannakis¹, Paola de Michelis⁵, Giuseppe Consolini⁶, Jesper Gjerloev⁷,
Lorenzo Trenchi⁸

¹IAASARS National Observatory of Athens, Athens, Greece

²Department of Physics, National & Kapodistrian University of Athens, Athens, Greece

³Space Applications & Research Consultancy, SPARC G.P., Athens, Greece

⁴Hellenic Space Center, Athens, Greece

⁵Istituto Nazionale di Geofisica e Vulcanologia, Rome, Italy

⁶INAF Istituto di Astrofisica e Planetologia Spaziali, Rome, Italy

⁷Johns Hopkins University Applied Physics Laboratory, USA

⁸ESRIN, European Space Agency, Italy

Key Points:

- New geomagnetic activity indices based on Swarm magnetic field data are computed similar to standard ground-based indices of Dst, ap and AE
- Swarm-derived indices show excellent correlations with both the traditional and SuperMAG-derived indices
- Swarm-based AE index enable us to monitor substorm activity also at the southern hemisphere

Corresponding author: Constantinos Papadimitriou, constantinos@noa.gr

This article has been accepted for publication and undergone full peer review but has not been through the copyediting, typesetting, pagination and proofreading process, which may lead to differences between this version and the [Version of Record](#). Please cite this article as [doi: 10.1029/2021JA029394](https://doi.org/10.1029/2021JA029394).

This article is protected by copyright. All rights reserved.

Abstract

Ground-based indices, such as the Dst, ap and AE, have been used for decades to describe the interplay of the terrestrial magnetosphere with the solar wind and provide quantifiable indications of the state of geomagnetic activity in general. These indices have been traditionally derived from ground-based observations from magnetometer stations all around the Earth. In the last 7 years though, the highly successful satellite mission Swarm has provided the scientific community with an abundance of high quality magnetic measurements at Low Earth Orbit (LEO), which can be used to produce the space-based counterparts of these indices, such the Swarm-Dst, Swarm-ap and Swarm-AE indices. In this work, we present the first results from this endeavour, with comparisons against traditionally used parameters. We postulate on the possible usefulness of these Swarm-based products for a more accurate monitoring of the dynamics of the magnetosphere and thus, for providing a better diagnosis of space weather conditions.

Plain Language Summary

Ground-based geomagnetic activity indices have been used for decades to monitor the dynamics of the Earth's magnetosphere, and provide information on two major types of space weather phenomena, i.e., magnetic storm and magnetospheric substorm occurrence and intensity. This study demonstrates how magnetic field data from a Low Earth Orbit (LEO) satellite mission, like ESA's Swarm constellation, can be used to derive corresponding space-based geomagnetic activity indices. Swarm is unravelling one of the most mysterious aspects of our planet: the magnetic field. The magnetic field and electric currents in and around our planet generate complex forces that have immeasurable impact on everyday life. The comparison of Swarm-based with ground-based indices shows a very good agreement, indicating that Swarm magnetic field data can be used to provide new satellite-based global indices to monitor the level of geomagnetic activity. Given the fact that the official ground-based index for the substorm activity is constructed by data from 12 ground stations solely in the northern hemisphere, it can be said that this index is predominantly northern, while the Swarm-derived substorm activity index may be more representative of a global state, since it is based on measurements from both hemispheres.

1 Introduction

The magnetosphere is a highly complex system of fields and currents that envelop the Earth and interact with each other producing a wide range of phenomena. One particular current system that holds special importance is the aptly named ring current. The ring current is a toroidal electric current flowing around the Earth, formed by the azimuthal motion of electrons and ions, extending from 3 to 8 Earth radii on the magnetospheric equatorial plane (Daglis et al., 1999). Because of its shape and direction, it forms its own magnetic field component, with an axis almost parallel to that of the Earth's dipole and the same polarity (southward). A direct consequence of this is that on the surface of our planet the ring currents induced magnetic field is opposite to the Earth's magnetic field. Thus, in cases where the incoming solar wind has the appropriate properties, e.g. in terms of velocity, and/or dynamic pressure, to cause particle injection in the inner magnetosphere and enhance the ring current, the terrestrial field on the surface of the planet will exhibit a decrease due to the increase of the counteracting ring current field. This is the phenomenon known as geomagnetic (or simply magnetic) storm, which seriously affects the electromagnetic environment of the Earth and can cause a wide range of significant effects ranging from telecommunication issues and satellite failures to the induction of high voltage electrical currents on electrical wires and conducting materials on the surface of the planet (Bothmer and Daglis, 2007). The monitoring of geomagnetic storms has been traditionally accomplished by means of the Disturbance storm-

71 time (Dst) index, which represents the axially symmetric disturbance of the horizontal
72 component of the magnetic field at the magnetic equator on the Earth's surface (Sugi-
73 iura and Kamei, 1981). As such, it operates as a proxy for the enhancement and sub-
74 sequent weakening of the ring current and hence the onset and evolution of magnetic storms.
75 Although Dst is the most well-known and used index, in this study we chose to use the
76 very similar SYM-H index (symmetric disturbance field in the horizontal direction H),
77 which is essentially the same as Dst (Sugiura and Poros, 1971), although it is built on
78 1 minute data from different stations and using a slightly different coordinate system.
79 SYM-H also represents the magnitude of the uniform field parallel to the dipole axis gen-
80 erated by the ring current and thus its interpretation remains the same as that for Dst.

81 Another group of current systems that cause an array of spectacular phenomena
82 are the auroral electrojets, which are currents that flow in concentrated channels of high
83 conductivity in the Earth's ionosphere and are carried by particles that generate the au-
84 roral light, moving both eastward (therefore forming the East ElectroJet EEJ) and west-
85 ward (therefore forming the West ElectroJet WEJ). Related to these systems are the
86 disturbances known as magnetospheric substorms (Akasofu, 1964; McPherron, 1979),
87 which are collective phenomena, considered as one of the major ways for the discharge
88 of accumulated energy in the terrestrial magnetosphere (Chian and Kamide, 2007). Dur-
89 ing the onset of substorm expansion phase, a dynamical process in the near Earth mag-
90 netosphere causes cross tail current to be diverted into the ionosphere, forming a sub-
91 storm current wedge consisting of downward (upward) field aligned currents on the dawn-
92 side (duskside) of the wedge and a westward auroral electrojet in the ionosphere (Kepko
93 at al., 2015). The Auroral Electrojet index AE (Davis and Sugiura, 1966) actually mea-
94 sures the intensity of this substorm enhanced westward ionospheric electrojet via its dia-
95 magnetic result on the horizontal component of the terrestrial magnetic field.

96 Balasis et al. (2019) recently derived a 1 Hz Swarm Dst-like index based solely on
97 magnetic data from the Swarm mission. The scientific merit of such a geomagnetic ac-
98 tivity index relies on its global character (since the three satellites provide a global Earth
99 coverage both latitudinally and longitudinally), as well as their proximity to the region
100 of emergence and activity of ionospheric currents. The present work further expands upon
101 that first effort, by simplifying and at the same time generalizing the approach so that
102 all three most commonly used indices of geomagnetic activity can be derived, namely
103 Dst (or SYM-H), ap (or Kp) and AE. Given the fact that the official ground-based AE
104 is constructed by data from 12 ground stations solely in the northern hemisphere and
105 the official ground-based ap from only 2 stations in the southern hemisphere (and 11 in
106 the northern one), it can be said that both of these indices are predominantly northern,
107 while the Swarm-derived AE and ap indices may be more representative of a global state,
108 since they are based on measurements from both hemispheres.

109 This article is divided upon 6 sections. Following the Introduction, Section 2 presents
110 the main steps of analysis and pre-processing of Swarm data that must be taken before
111 the method is applied, as well as the argumentation on the selection of an appropriate
112 time interval for the demonstration of the effectiveness of the methods. Section 3 out-
113 lines the new process for the derivation of the Swarm-Dst index and is complemented
114 by a comparison against the standard Dst index. The same line of thinking is followed
115 in Sections 4 and 5, correspondingly for the ap and AE indices, while Section 6 summa-
116 rizes the findings and offers some general remarks on the usefulness of the method.

117 2 Data Selection and Pre-processing

118 Our explorers in this quest for an ever more detailed description of the Earth's mag-
119 netic field are the satellites of the Swarm constellation (Friis-Christensen et al., 2006).
120 Swarm is the fifth mission in ESA's fleet of Earth Explorers, aspiring to carry out the
121 most accurate and detailed description of the Earth's magnetic field. Launched on 23

122 November 2013, the mission is composed of three satellites in polar Low-Earth Orbit (LEO),
123 with two of them (Swarm-A and Swarm-C) flying side by side at an initial altitude of
124 460 km and the third (Swarm-B) flying slightly higher at 510 km. Carrying highly pre-
125 cise instruments, the mission offers the most up-to-date survey of the terrestrial mag-
126 netic field (De Michelis et al., 2015; Hulot et al., 2015; Olsen et al., 2015), but also of
127 the general near-Earth electromagnetic environment and its interaction with the solar
128 wind (Balasis et al., 2015; Olsen et al., 2016; Papadimitriou et al., 2018).

129 The derivation of the Swarm indices is based on the dataset prepared within the
130 framework of the INTENS (Characterization of IoNospheric Turbulence level by Swarm
131 constellation) project. The dataset was constructed from the Level 1b, MAG_LR prod-
132 uct of the Swarm mission (<https://swarm-diss.eo.esa.int/>), which contains among oth-
133 ers, magnetic field measurements from the Vector Field Magnetometer (VFM) instru-
134 ment (Tffner-Clausen et al., 2016) on board the three satellites at a time sampling of 1
135 second. The magnetic field measurements are given as a three-dimensional vector in the
136 North-East-Center coordinate system, with its origin being the VFM instrument itself.
137 The static, background field was subtracted from these by removing the internal mode
138 of the CHAOS-6 model (Finlay et al., 2016), which consists of the core and crustal mag-
139 netic field contributions of the Earth. The residuals are then mapped to the Quasi-Dipole
140 coordinate system (Emmert et al., 2010). From there, it is easy to map the vector to a
141 mean Field Aligned (MFA) coordinate system, by taking the projection of the total vec-
142 tor field on a direction that is parallel to the main, internal model field, thus construct-
143 ing the B_{par} component and two perpendicular components B_{per1} and B_{per2} . The lat-
144 ter two are constructed so that B_{per1} is mostly along the meridional plane pointing out-
145 wards and B_{per2} mainly along the East-West direction pointing Eastwards. Obvious out-
146 liers, i.e. isolated spikes, were removed by applying a simple threshold and as a final step,
147 the magnitude of the residual vector was computed and saved for further processing.

148 The time period that we selected for the illustration of the method was the year
149 of 2015, which is appropriate to test the Swarm indices during both quiet and disturbed
150 geomagnetic conditions. Indeed, 2015 was characterized by two months of intense ge-
151 omagnetic activity due to the storms of March 17th and June 23rd, two events that have
152 been extensively discussed by the scientific community (Liu et al., 2015; Kataoka et al.,
153 2015; Wang et al., 2016; Wu et al., 2016; Marubashi et al., 2016; Balasis et al., 2018; De
154 Michelis et al., 2020), as well as a third event of less intensity, yet still an important one,
155 the storm of the 22nd of December. Additionally, several substorms erupted between and
156 following the storm events, which had shorter duration and thus were interspersed by
157 several quiet intervals as well. As such, this period provides a blend of both storm and
158 substorm activity, while also exhibiting intervals of quiescence and is perfectly suited for
159 modelling all levels of geomagnetic activity.

160 A year-long duration is also important to achieve complete coverage in all local times
161 (LT), given the slow rotation of the orbital plane of the satellites with respect to the Sun-
162 Earth line. Specifically for 2015, Swarm-A required approximately 136 days for its or-
163 bital plane to complete a 180° rotation, while Swarm-B, being at slightly higher altitude
164 and thus slower, required a little longer, approximately 146 days. Since the satellites are
165 on the day-side for the first half of their orbit and on the night-side for the other, a 180°
166 rotation provides full local time coverage. The time spent by the Swarm satellites in each
167 bin of Magnetic Local Time (MLT) is shown in Figure 1 (only one of the satellites of the
168 lower pair is shown, Swarm-A and not Swarm-C, since their orbits are almost identical).
169 Additionally, by selecting such a time period, the faster, local and MLT-constrained vari-
170 ations will sometimes be located in MLTs that are covered by the satellites and some-
171 times not, thus ensuring a proper validation of the outputs. To complement this image,
172 the number of measurements in bins of magnetic latitude is given in Figure 2. As can
173 be seen, by selecting a full year of data both Swarm-A and Swarm-B provide full geo-
174 graphical coverage, despite the small differences in orbital characteristics.

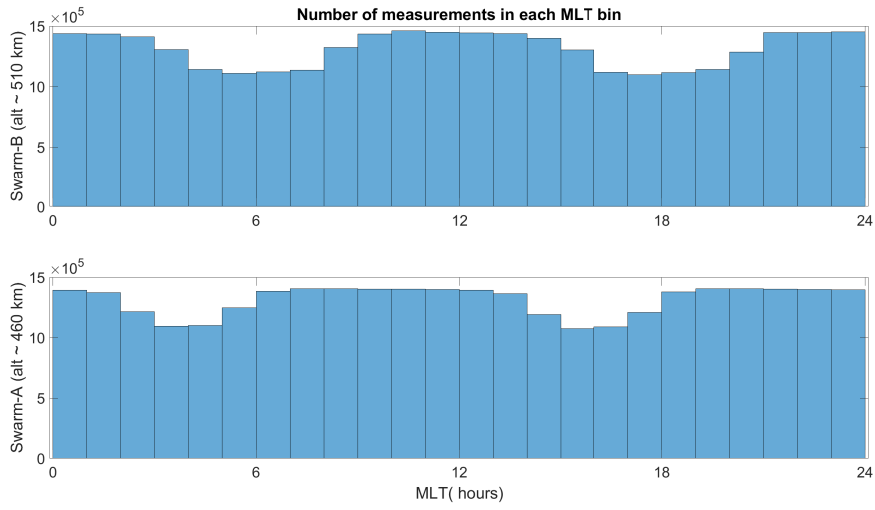


Figure 1. Number of measurements performed by the Swarm satellites in each MLT bin. Top panel shows Swarm-B and bottom panel Swarm-A (Swarm-C is identical).

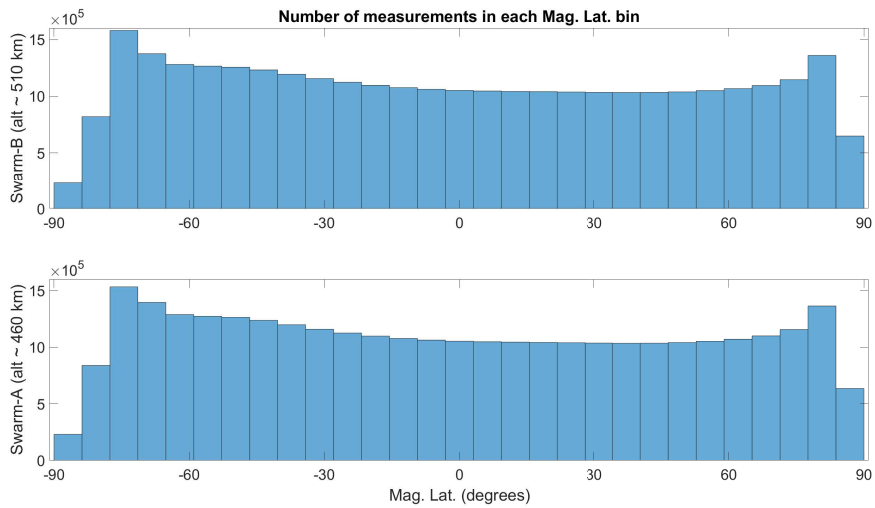


Figure 2. Number of measurements performed by the Swarm satellites in each Mag. Lat. bin. Top panel shows Swarm-B and bottom panel Swarm-A (Swarm-C is identical).

3 The Swarm-derived Dst Index

Magnetic storms produce global magnetic disturbances on the Earth's surface, which serve as the basis for storm monitoring via the hourly Dst index. It is derived from the variations of the horizontal component of the terrestrial magnetic field, using data from four observatories, positioned at magnetic latitudes ranging from approximately -30° to $+30^\circ$. The derivation process includes the baseline definition based on the five quietest days of each month for each observatory and the subtraction of the resulting annual mean values of the horizontal component from the observed ones. The solar quiet daily variation, Sq, is also determined and removed, resulting in the disturbance variation for each observatory, which is then averaged over the four observatories and normalized to the dipole equator, thus producing the Dst index [<http://wdc.kugi.kyoto-u.ac.jp/dstdir/dst2/onDstindex.html>].

The derivation procedure of the SYM-H index is similar to the Dst one; it includes the subtraction of the geomagnetic main field and the Sq to calculate the disturbance field component, a coordinate transformation to a dipole coordinate system and finally the calculation of both the longitudinally symmetric (SYM-H and SYM-D) components, by averaging the disturbance component at each minute for the 6 selected stations (Iyemori et al., 2010). Thus, the SYM-H index is being produced with a 1-minute sampling time and can capture the storm-related effects with a much higher temporal resolution. Due to this, we used SYM-H index data from the World Data Center for Geomagnetism at kyoto, Japan for the derivation of the Swarm-based index and thus were able to also produce a 1-minute cadence index.

In order to mirror the behaviour of the ground station data, it is imperative to remove measurements that were performed when the satellites were at high latitudes. Thus, the first step in the process is to discard times where the satellites were above $+30^\circ$ or below -30° in magnetic latitude. At those near-equatorial latitudes, a good proxy for the horizontal component of the terrestrial magnetic field is the B_{par} , so the process continues keeping only this component and ignoring the others. Unfortunately, keeping only measurements within specific latitudes unavoidably means that, for certain times, none of the satellites will be within the prescribed latitudinal limits and thus, gaps will be present in the series. For certain cases even as much as half the time series may be empty, with the duration of the gaps ranging almost uniformly from a few seconds up to half an hour. To somehow alleviate this, a non-overlapping, moving average scheme is applied on the time series, with a window of 60 seconds, so that the series are now set to a 1-minute time resolution, effectively filling-up some of the smaller gaps. Up to this point, the analysis was performed separately for each of the satellites Swarm-A and Swarm-B, while Swarm-C having almost the same orbit as Swarm-A, at the same altitude, lagging behind it by just 5 to 10 seconds and being separated by only 1.4 degrees in longitude, yields the same results as A so it was not used. In the next step the two series are merged, in a joint 1-min resolution dataset, so that if both satellites are concurrently within the latitude limits their values are averaged, otherwise we keep only the ones from the satellite that was within the prescribed latitudes. The remaining gaps are interpolated using a simple linear scheme, to produce a complete time series. Then, a low-pass, Chebyshev Type I filter is used, with a cutoff period of 4 hours, to filter out some of the small perturbations in the signal that arise from the fast motion of the satellites. Finally, we apply a linear transform of the form:

$$S_{Dst} = 1.53B_f + 12.85$$

where B_f is the filtered series acquired in the last step, to get the final Swarm-Dst index S_{Dst} . A flowchart of the method, showing the form of the time series at each intermediate step described here is shown in Figure 3. A comparison of the final Swarm index against the ground-based SYM-H is shown in Figure 4, where it is evident how this method can produce an index that is strikingly similar to the traditionally used one, a

226 similarity that is justified by a Pearson correlation coefficient (Pearson, 1895) of 0.94 be-
 227 tween the two. We have named the index Swarm-Dst instead of Swarm-SYM-H purely
 228 for convenience, since we believe Dst to be the one of the two which more scientists have
 229 used and are familiar with, but the results remain practically the same when compar-
 230 ing the Swarm-derived index against Dst as well.

231 A first attempt to produce a Swarm-derived Dst index was performed in 2019, by
 232 Balasis et al., but the parameters of the method then were mostly empirically derived
 233 and it was only used for Dst. In this study, the process is simplified and at the same time
 234 generalized, so that it can be used to produce other indices as well, with only a change
 235 of the four parameters, which are the latitudinal limits, the filtering cutoff and the two
 236 parameters of the linear transform. Even though their choice is intuitive in this case, a
 237 more formal derivation is achieved by following two simple steps, which also apply for
 238 the two following cases of the Swarm-based ap and AE indices. First, many different com-
 239 binations for the latitudes and filtering cutoff are tested, trying to find the one that max-
 240 imizes the correlation with the ground-based index series and secondly, keeping the first
 241 two constant, we find the linear transform parameters that minimize the root mean square
 242 error between the filtered series and the standard index. Thus, the results that we present,
 243 both here as well as in the two cases that follow, are the best found after a long series
 244 of tests and tweaking of the parameter values. An issue that is not addressed with the
 245 present methodology is the removal of the effect of the Sq current, which for a moving,
 246 satellite observatory cannot be performed with the same manner that is calculated for
 247 ground stations, but which could be attempted in a future work, using methods inspired
 248 from other Level-2 products from the Swarm mission (Alken et al., 2015).

249 4 The Swarm-derived ap Index

250 The geomagnetic three-hourly Kp index was introduced by J. Bartels in 1949 and
 251 is derived from 13 magnetic observatories, 11 of which in the Northern Hemisphere, be-
 252 tween latitudes from +38° up to +60° and 2 in the Southern Hemisphere at latitudes
 253 of -43° and -35°. The derivation of the Kp index includes the removal of the quiet-day
 254 variation pattern before the local disturbance levels are determined from the difference
 255 between the highest and lowest values (range) during 3-hourly time intervals for the most
 256 disturbed horizontal magnetic field component. The range is then converted into a lo-
 257 cal K index, which by statistical methods is converted to a standardized index, Ks, con-
 258 sisting of twenty eight values. Global Kp index is the average of the local Ks indices. [[https://www.gfz-
 259 potsdam.de/en/kp-index/](https://www.gfz-potsdam.de/en/kp-index/)]. It is designed to measure solar particle radiation by its mag-
 260 netic effects and today it is considered a proxy for the energy input from the solar wind
 261 to Earth. The name Kp was derived from the German words “planetarische Kennziffer
 262 meaning “planetary index. The index is quasi-logarithmic in nature and since this is more
 263 difficult to assign to actual magnetic field measurements, Bartels also proposed a cor-
 264 respondence between Kp values and the more linear ap index values. Due to this, we will
 265 also use the ap index for this study, keeping in mind that a simple one-to-one relation
 266 can map the ap values to Kp and vice-versa. Since no better time resolution form of the
 267 data exists other than the default 3-hour one, the series were linearly interpolated to a
 268 1-minute cadence to allow us to generate the corresponding Swarm-based index at the
 269 same resolution as for the previous case.

270 We repeat the exact same process as above, tweaking the four parameters until the
 271 best possible outcome emerges. For the Swarm-ap index we use measurements of the mag-
 272 nitude of the residual field vector, located in a narrow band between +55° and +60° in
 273 the Northern Hemisphere and correspondingly -60° to -55° in the Southern one, which
 274 despite being so restricted was the only latitudinal choice from a wide range of values
 275 tested, that produced the best result. The cutoff period is set to 9 hours and the linear
 276 transform to $S_{ap} = 0.39B_f - 4.29$ in order to achieve a maximum correlation coeffi-
 277 cient of 0.86. The sampling time of the new series has been set to 1 minute, as for the

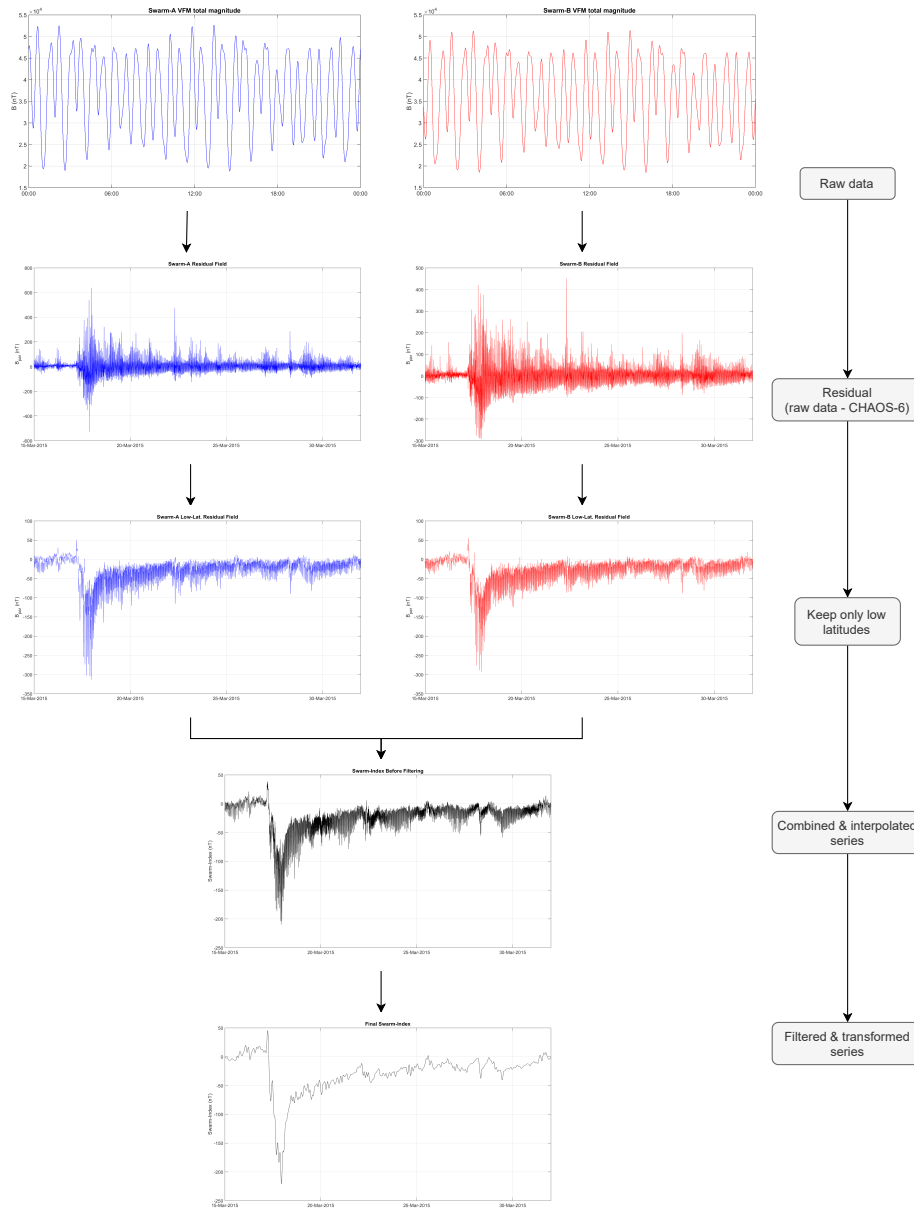


Figure 3. Flowchart for the derivation of the Swarm-Dst index. Each of the 3 upper rows includes distinct panels for Swarm-A (blue) and Swarm-B (red) time series, while each of the next 2 rows shows a single panel of combined Swarm-A and Swarm-B time series.

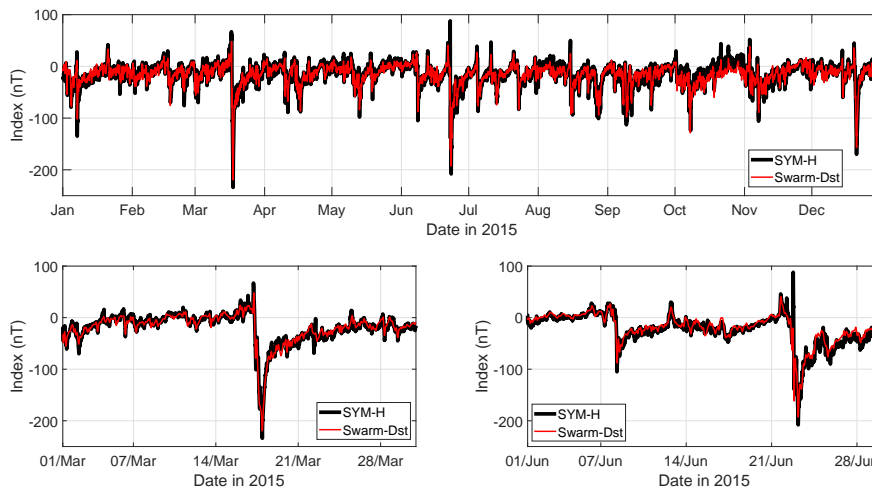


Figure 4. Swarm-derived Dst index (red) compared to the ground-based SYM-H index (black). Top panel shows the entire 12 month period from Jan 1st to Dec 31st 2015, while the two bottom panels show zoomed pictures for March (bottom left) and June 2015 (bottom right).

Swarm-Dst case. The result is shown in Figure 5. As can be seen the Swarm index closely follows the standard ap index, missing only in absolute magnitude a few of the highest peaks. This hints at the possibility of a non-linear transform which would promote high values more significantly than the lower ones, something which makes sense given the peculiar way with which these indices are produced.

5 The Swarm-derived AE Index

The AE index represents the overall activity of the electrojets. The AE index is derived from geomagnetic variations in the horizontal component observed at selected observatories along the auroral zone, solely in the Northern Hemisphere, at magnetic latitudes between $+60^\circ$ and $+70^\circ$. The derivation process includes the data normalization, by averaging all the data on the five international quietest days, thus calculating a base value for each station for each month. This base value is subtracted from each 1-min value obtained at the station during that month. Then among the data from all the stations at each given time (UT), the largest and smallest values are selected, defining the AU and AL indices. Their difference defines the AE index. [<http://wdc.kugi.kyoto-u.ac.jp/aedir/ae2/onAEindex.html>]

To mirror this we follow the same process outlined above, again for the magnitude of the residual field, keeping only measurements between $+65^\circ$ and $+75^\circ$ (and correspondingly -75° to -65°) in magnetic latitude, filtering with a cutoff period of 2.6 hours and applying the transform $S_{AE} = 2.2B_f - 8.9$, with all of these parameter choices made after several values were tested to achieve a maximum correlation coefficient of 0.85, again for a time series of 1-minute resolution. As can be seen in Figure 6, while the Swarm index doesn't match the peaks during the intense storm events, it captures with high accuracy the substorm activity during April and May, highlighted with the two bottom panels which zoom in two characteristic intervals. The discrepancies could possibly be alleviated with the application of a non-linear transform, which could hint at the inherent non-linear relationship of the parameters involved, between ground and Swarm altitudes, or between the different methodologies by which both indices have been produced. It should also be noted that despite trying to more faithfully imitate the derivation of the ground index, by first estimating the Swarm-AL and Swarm-AU indices and deriving Swarm-AE

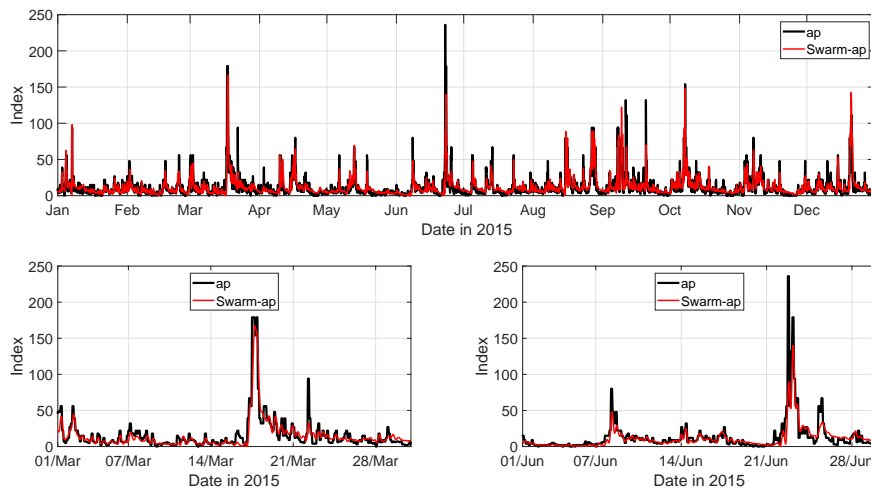


Figure 5. Swarm-derived ap index (red) compared to the standard index (black). Top panel shows the entire 12 month period from Jan 1st to Dec 31st 2015, while the two bottom panels show zoomed pictures for March (bottom left) and June 2015 (bottom right).

as their difference, the results were consistently poorer, so we opted in favour of the method described above.

One of the most important benefits of using a satellite observatory is that by slightly changing the formulation of the method, one can easily produce more localized versions of these indices. As an example, by imposing the latitudinal limits to only maintain measurements from the north or the south hemisphere, while keeping the rest of the method unchanged, we can construct the Swarm-AE-North and Swarm-AE-South indices, to complement the full version of Swarm-AE. This is shown in Figure 7, where the full Swarm-AE index is overplotted by its localized North and South hemisphere counterparts. Even though the two localized indices agree, in general, with each other, if we draw our attention to specific, small intervals, like the ones depicted on the two bottom subplots of Figure 7, one can see small, but significant differences between the two. This comes as a verification of recent literature (Liou et al., 2018) in which they report that substorm onset is far from north-south symmetric, as was previously considered, and that it is more likely to be initiated in a dark than a sunlit oval. They additionally showed that the preferred locations of substorm onsets coincide with the local peak of the Earth's magnetic field (or a minimum in the ionospheric conductivity), a finding which is consistent with an ionospheric feedback mechanism. Similar asymmetries were also reported by Weygand et al. (2014) based on magnetic field data from ground based observatories.

6 Comparisons against SuperMAG Indices

There has been a huge effort in recent years to complement the traditional indices of geomagnetic activity with new versions, utilizing data from the immense ground magnetometer network SuperMAG. SuperMAG is a worldwide collaboration of organizations and national agencies which currently operate more than 300 ground-based magnetometers spread across the globe (Gjerloev, 2009). Data from each of these stations are processed according to the same guidelines (Gjerloev, 2012) and utilized, according to their latitudinal location to produce the SuperMAG geomagnetic activity indices: the SMR index, which is a ring current index, similar to Dst or SYM-H (Newell et al., 2012) and

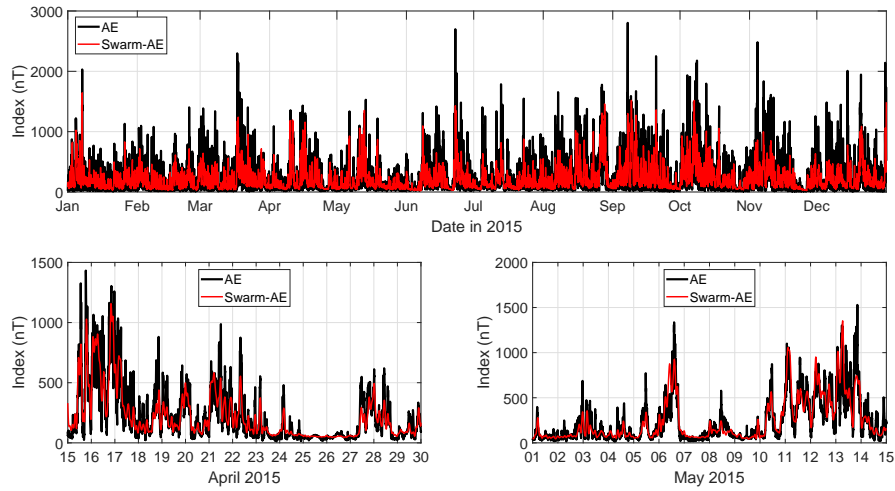


Figure 6. Swarm-derived AE index (red) compared to the standard AE index (black). Top panel shows the entire 12 month period from Jan 1st to Dec 31st 2015, while the two bottom panels show zoomed pictures from the second half of April (bottom left) and first half of May (bottom right).

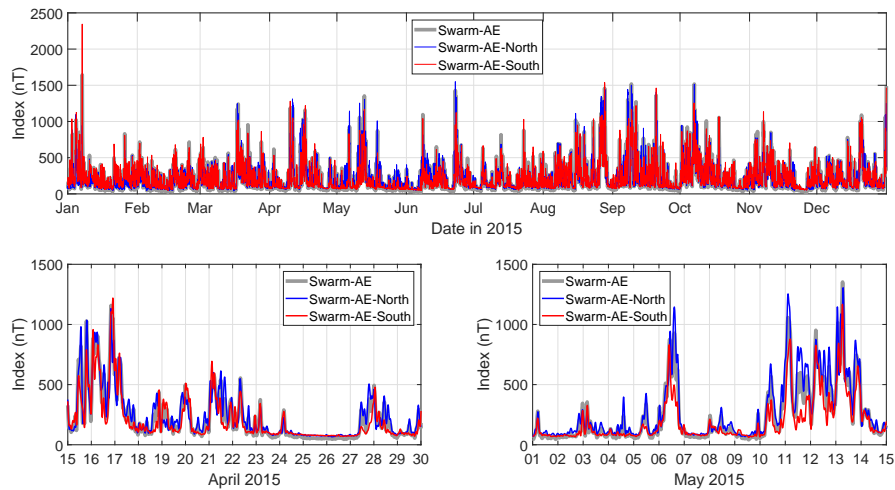


Figure 7. Swarm-derived AE index (grey) compared to its regional counterparts the Swarm-AE-North (blue) and Swarm-AE-South (red) indices. Top panel shows the entire 12 month period from Jan 1st to Dec 31st 2015, while the two bottom panels show zoomed pictures from the second half of April (bottom left) and first half of May (bottom right).

Table 1. Summary of results

Correlations with ring current indices	
Swarm-Dst vs SYM-H	0.94
Swarm-Dst vs SMR	0.95
Correlations with ap index	
Swarm-ap vs ap	0.86
Correlations with auroral electrojet indices	
Swarm-AE vs AE	0.85
Swarm-AE vs SME	0.86
Swarm-AE-North vs AE	0.81
Swarm-AE-South vs AE	0.77

the SME index, which attempts to capture the auroral electrojet behavior and thus operate in a manner analogous to the AE index (Newell et al., 2011). Both of these, as well as other relevant products, are available from the SuperMAG website at a temporal resolution of 1 minute. As a first step to incorporate these new indices in our work, we performed two simple comparisons, calculating the correlation coefficient between the Swarm-Dst and the SuperMAG SMR index, which yielded a value of 0.95 and also compared Swarm-AE (the full version) against SuperMAG SME, which gave the result 0.86. Both of these values are slightly higher than the ones procured by comparisons against the traditional SYM-H and AE indices, which indicates that the satellite indices are closer to the new indices, which are more detailed and are being produced by many more observatories than the old ones, although further work is needed to address these differences properly. That being said, this is a very promising result that we believe further justifies our approach and opens new avenues for exploration.

These results, along with all the previous ones, are presented in Table 1, while a pictorial representation of this comparison is shown in Figure 8.

7 Discussion and Conclusions

This work shows how the magnetic field data from the Swarm mission can be utilized, by means of a simple and intuitive method to reproduce, with high accuracy, the three major indices of geomagnetic activity, namely the Dst, ap (or Kp) and AE indices. The global coverage provided by a constellation of low-Earth orbiting satellites makes them ideal for encapsulating the entirety of the magnetic field, discerning changes at larger spatial scales, while their altitude positions them right in the place of the ionospheric currents which are responsible for many of the effects that comprise our notion of space weather. We note that the Swarm AE-like index could, in principle, be more representative of a global state, since it is based on measurements from both hemispheres, while the ground-based one is computed from measurements in the Northern Hemisphere only.

Additionally, since the satellites remain at fairly constant LTs for several weeks, their data can further promote recent research on regional indices of electrojet or ring current activity, such as the regional versions of SME and SMR indices (Bergin et al., 2020). As such, satellite magnetic observatories can complement their ground-based counterparts, providing new insights into the state of the magnetosphere and new promise for more accurate diagnosis of space weather conditions.

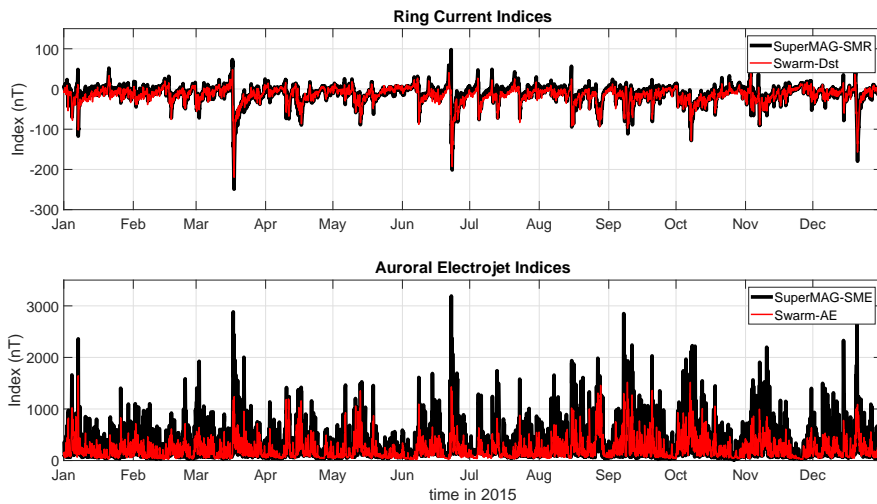


Figure 8. Comparisons of SuperMAG indices (with black) SMR (top panel) and SME (bottom panel) against their Swarm-derived counterparts (with red) for the year 2015.

Acknowledgments

The results presented rely on data collected by the three satellites of the Swarm constellation. We thank the European Space Agency (ESA) that supports the Swarm mission. Swarm data can be accessed at <https://swarm-diss.eo.esa.int/>. We acknowledge the Kyoto World Data Center (WDC) for Geomagnetism and the observatories that produce and make Dst, SYM-H and AE indices available at <http://wdc.kugi.kyoto-u.ac.jp/> and the GFZ German Research Centre for Geosciences for producing and providing ap, Kp and all other relevant indices at <https://www.gfz-potsdam.de/en/kp-index/>. We gratefully acknowledge the SuperMAG collaborators for the provision of ground-based index data (<https://supermag.jhuapl.edu/info/?page=acknowledgement>). The authors acknowledge financial support from European Space Agency (ESA contract N. 4000125663/18/INB “EO 486 Science for Society Permanently Open Call for Proposals EOEP-5 BLOCK4” (INTENS)). This work was benefited from discussions within the International Space Science Institute (ISSI) Team # 455 “Complex Systems Perspectives Pertaining to the Research of the Near-Earth Electromagnetic Environment”.

References

- Akasofu, S.-I. (1964). The development of the auroral substorms. *Planet. Space Sci.*, 12, 273.
- Alken, P., S. Maus, A. Chulliat, P. Vigneron, O. Sirol and G. Hulot (2015). Swarm equatorial electric field chain: first results, *Geophys. Res. Lett.*, 42, 673680, doi:10.1002/2014GL062658.
- Balasis, G., Papadimitriou, C., Daglis, I. A., and Pilipenko, V. (2015). ULF wave power features in the topside ionosphere revealed by Swarm observations. *Geophys. Res. Lett.*, 42, 6922-6930, doi:10.1002/2015GL065424.
- Balasis, G., et al. (2018). Observation of intermittency-induced critical dynamics in geomagnetic field time series prior to the intense magnetic storms of March, June, and December 2015. *J. Geophys. Res.: Space Phys.*, 123, 4594-4613, doi:10.1002/2017JA025131.
- Balasis, G., Papadimitriou, C., and Boutsis, A. Z. (2019). Ionospheric response to solar and interplanetary disturbances: a Swarm perspective. *Philosophical*

- 397 *Transactions A*, doi:10.1098/rsta.2018.0098.
- 398 Bartels, J. (1949). The standardized index Ks and the planetary index Kp. *IATME*
399 *Bull.* 12 (b), 97, IUGG Publ.
- 400 Bothmer, V., and Daglis, I. A. (2007). In V. Bothmer and I. A. Daglis (Eds.), *Space*
401 *Weather: Physics and Effects*, Praxis/Springer, New York, (438 pp.), ISBN
402 978-3-540-23907-9.
- 403 Bergin, A., Chapman, S., and Gjerloev, J. (2020). AE, Dst and their SuperMAG
404 Counterparts: The Effect of Improved Spatial Resolution in Geomagnetic
405 Indices. *J. Geophys. Res.: Space Physics*, 125, doi:10.1029/2020JA027828.
- 406 Chian, A. C.-L., and Kamide, Y. (2007). An Overview of the Solar-Terrestrial En-
407 vironment. In Y. Kamide and A. C.-L. Chian (Eds.), *Handbook of the Solar-*
408 *Terrestrial Environment*, Springer-Verlag, Berlin, Heidelberg, doi:10.1007/978-
409 3-540-46315-3.
- 410 Daglis, I. A., Thorne, R. M., Baumjohann, W., and Orsini, S. (1999). The terres-
411 trial ring current: Origin, formation, and decay. *Rev. Geophys.*, 37(4), 407-438,
412 doi:10.1029/1999RG900009.
- 413 Davis, T. N., and Sugiura, M. (1966). Auroral electrojet activity index AE
414 and its universal time variations. *J. Geophys. Res.*, 71(3), 785801,
415 doi:10.1029/JZ071i003p00785.
- 416 De Michelis, P., Consolini, G., and Tozzi, R. (2015). Magnetic field fluctuation fea-
417 tures at Swarms altitude: A fractal approach. *J. Geophys. Res.*, 42, 31003105,
418 doi:10.1002/2015GL063603.
- 419 De Michelis, P., Pignalberi, A., Consolini, G., Coco, I., Tozzi, R., and Pezzopane,
420 M., et al. (2020). On the 2015 St. Patrick's storm turbulent state of the iono-
421 sphere: Hints from the Swarm mission. *Journal of Geophysical Research: Space*
422 *Physics*, 125, e2020JA027934. <https://doi.org/10.1029/2020JA027934>
- 423 Emmert A. D., D. P. Richmond, and D. P. Drob (2010), A computationally compact
424 representation of magnetic apex and quasi dipole coordinates with smooth
425 base vectors, *J. Geophys. Res.*, 115, doi:10.1029/2010JA015326.
- 426 Finlay, C., et al. (2016). Recent geomagnetic secular variation from Swarm and
427 ground observatories as estimated in the CHAOS-6 geomagnetic field model.
428 *Earth Planets and Space*, 68, 112, doi:10.1186/s40623-016-0486-1.
- 429 Friis-Christensen, E., Lhr, H., and Hulot, G. (2006). Swarm: A constellation
430 to study the Earth's magnetic field. *Earth Planets Space*, 58, 351358,
431 doi:10.1186/BF03351933.
- 432 Gjerloev, J. W. (2009). A global ground-based magnetometer initiative. *Eos Trans.*
433 *AGU*, 90 (27), 230231, doi:10.1029/2009EO270002.
- 434 Gjerloev, J. W. (2012). The SuperMAG data processing technique. *J. Geophys. Res.*,
435 117, A09213, doi:10.1029/2012JA017683.
- 436 Hulot, G., Vigneron, P., Lger, J.-M., Fratter, I., Olsen, N., Jager, T., Bertrand,
437 F., Brocco, L., Sirol, O., Lalanne, X., Boness, A., and Cattin, V. (2015).
438 Swarms absolute magnetometer experimental vector mode, an innovative
439 capability for space magnetometry. *Geophys. Res. Lett.*, 42, 1352-1359,
440 doi:10.1002/2014GL062700.
- 441 Iyemori, T., Takeda, M., Nose, M., Odagi, Y., and Toh, H. (2010). Mid-latitude
442 Geomagnetic Indices ASY and SYM for 2009 (Provisional). In *Internal Re-*
443 *port of Data Analysis Center for Geomagnetism and Space Magnetism*, Kyoto
444 University, Japan.
- 445 Kataoka, R., et al. (2015). Pileup accident hypothesis of magnetic storm on 17
446 March 2015. *Geophys. Res. Lett.*, 42, 5155-5161, doi:10.1002/2015GL064816.
- 447 Kepko, L., McPherron, R. L., Amm, O., et al. (2015). Substorm Current Wedge
448 Revisited. *Space Sci Rev*, 190, 1-46, doi:10.1007/s11214-014-0124-9.
- 449 Liou, K., Sotirelis, T., and Mitchell, E. J. (2018). North-South Asymmetry in the
450 Geographic Location of Auroral Substorms correlated with Ionospheric Effects.
451 *Sci Rep* 8, 17230, doi:10.1038/s41598-018-35091-2.

- 452 Liu, Y. D., et al. (2015). Plasma and magnetic field characteristics of solar cor-
453 onal mass ejections in relation to geomagnetic storm intensity and variability.
454 *Astrophys. J. Lett.*, 809, L34, doi:10.1088/2041-8205/809/2/L34.
- 455 Marubashi, K., et al. (2016). The 17 March 2015 storm: the associated magnetic
456 flux rope structure and the storm development. *Earth Planets Space*, 68, 173,
457 doi:10.1186/s40623-016-0551-9.
- 458 McPherron, R. I. (1979). Magnetospheric substorms. *Rev. Geophys.*, 17, 657.
- 459 Newell, P. T., and Gjerloev, J. W. (2011). Evaluation of SuperMAG auroral electro-
460 jet indices as indicators of substorms and auroral power. *J. Geophys. Res.*, 116,
461 A12211, doi:10.1029/2011JA016779.
- 462 Newell, P. T., and Gjerloev, J. W. (2012). SuperMAG-Based Partial Ring Current
463 Indices. *J. Geophys. Res.*, 117, doi:10.1029/2012JA017586.
- 464 Olsen, N., Hulot, G., Lesur, V., Finlay, C. C., Beggan, C., Chulliat, A., Sabaka,
465 T. J., Floberghagen, R., Friis-Christensen, E., Haagmans, R., Kotsiaros, S.,
466 Lhr, H., Tffner-Clausen, L., and Vigneron, P. (2015). The Swarm Initial Field
467 Model for the 2014 geomagnetic field. *Geophys. Res. Lett.*, 42, 1092-1098,
468 doi:10.1002/2014GL062659.
- 469 Olsen, N., Stolle, C., Floberghagen, R., Hulot, G., and Kuvshinov, A. (2016). Special
470 issue Swarm science results after 2 years in space. *Earth Planets Space*, 68, 13,
471 doi:10.1186/s40623-016-0546-6.
- 472 Pearson, K. (1895). Notes on regression and inheritance in the case of two parents.
473 *P. R. Soc. London*, 58, 240-242.
- 474 Papadimitriou, C., Balasis, G., Daglis, I. A., and Giannakis, O. (2018). An initial
475 ULF wave index derived from two years of Swarm observations. *Ann. Geo-*
476 *phys.*, 36, 287-299, doi:10.5194/angeo-36-287-2018.
- 477 Sugiura, M., and Kamei, T. (1981). IAGA Bulletin N°40, [http://wdc.kugi.kyoto-](http://wdc.kugi.kyoto-u.ac.jp/dstdir/dst2/onDstindex.html)
478 [u.ac.jp/dstdir/dst2/onDstindex.html](http://wdc.kugi.kyoto-u.ac.jp/dstdir/dst2/onDstindex.html).
- 479 Sugiura, M., and D.J. Poros, Hourly values of equatorial Dst for years 1957 to 1970,
480 Rep. X-645-71-278, Goddard Space Flight Center, Greenbelt, Maryland, 1971.
- 481 Tffner-Clausen, L., Lesur, V., Olsen, N., and Finlay, C. (2016). In-flight scalar cal-
482 ibration and characterisation of the Swarm magnetometry package. *Earth,*
483 *Planets and Space*, 68(1), 129, doi:10.1186/s40623-016-0501-6.
- 484 Wang, Y., et al. (2016). On the propagation of a geoeffective coronal mass
485 ejection during 15–17 March 2015. *J. Geophys. Res.*, 121, 7423-7434,
486 doi:10.1002/2016JA022924.
- 487 Weygand, J. M., Zesta, E., and Troshichev, O. (2014), Auroral electrojet indices in
488 the Northern and Southern Hemispheres: A statistical comparison, *J. Geophys.*
489 *Res. Space Physics*, 119, 4819-4840, doi:10.1002/2013JA019377.
- 490 Wu, C. C., et al. (2016). The first super geomagnetic storm of solar cycle 24:
491 The St. Patrick's day event (17 March 2015). *Earth Planets Space*, 68, 151,
492 doi:10.1186/s40623-016-0525-y.